# In-Situ UV/vis and Transient Isotopic Analysis of the Role of Oxidizing Agent in the Oxidative Dehydrogenation of Propane over Silica-Supported Vanadia Catalysts

**Olga Ovsitser, Maymol Cherian, and Evgenii V. Kondratenko***

*Leibniz-Institut für Katalyse e. V. an der Universität Rostock, Aussenstelle Berlin (former ACA Berlin-Adlershof), Richard-Willstätter-Strasse 12 D-12489 Berlin, Germany*

*Received: January 29, 2007; In Final Form: April 12, 2007*

In-situ UV/vis spectroscopy in combination with transient isotopic analysis was applied for elucidating the governing factors, which determine the superior performance of $N_2O$ as compared to $O_2$ in the oxidative dehydrogenation of propane (ODP) over $VO_x$/MCM-41, $VO_x$/MCM-48, and $VO_x/SiO_2$ catalytic materials. Characterization studies applying in-situ steady-state UV/vis spectroscopy evidenced higher reduction degree of surface $VO_x$ species at 773 K in a $C_3H_8-N_2O$ ($C_3H_8/N_2O = 1/1$) feed than in a $C_3H_8-O_2$ ($C_3H_8/O_2 = 2/1$) flow at controlled conversions of propane (<5%) and oxidizing agent (<10%). The in-situ UV/vis method in a transient mode enabled to distinguish the ability of $O_2$ and $N_2O$ for reoxidation of reduced $VO_x$ species; $N_2O$ reoxidizes reduced $VO_x$ species slower than $O_2$. This property of $N_2O$ is very essential for suppressing nonselective consecutive propene oxidation to $CO_x$ (mainly to CO). Additionally, the results of transient isotopic experiments in the temporal analysis of products reactor revealed that adsorbed (nonlattice) oxygen species are formed upon $O_2$ activation over reduced $VO_x$ species and participate in $CO_2$ and CO formation. It is suggested that these nonselective species do not originate from $N_2O$.

## 1. Introduction

Oxidation reactions, that is, transformation of chemicals into various products in the presence of oxidizing agent, play an essential role in the modern industrial catalysis.[1,2] However, the developed processes are mainly based on the olefin chemistry. The achievements of oxidation catalysis in the field of oxidative transformation of alkanes (saturated hydrocarbons) to olefins or oxygenates are very modest. Therefore, this is still a challenging area of the modern oxidation catalysis. For propene formation, the industry is now faced with the problem of booming of propene demand from one side and low propene supply from another side. The oxidative dehydrogenation of propane (ODP) is considered to be an alternative to the existing industrial processes. The exothermicity of this reaction enables to operate at lower reaction temperatures than in the case of nonoxidative dehydrogenation processes. Moreover, the ODP reaction is thermodynamically not limited. Numerous catalytic systems have been evaluated for this reaction and the relevant results have been recently reviewed.[3,4] Promising catalyst formulations are based on relatively complex systems based on molybdenum and vanadium oxides. However, the main challenge is still to minimize the formation of carbon oxides ($CO_x$) that is favored at high degrees of propane conversion because of higher reactivity of propene as compared to propane. This results in the need to isolate the selective reaction products before side products are formed. The extent of kinetic isolation of the selective products depends on the relative rates of the formation of a specific selective product and the rates of its further conversion to $CO_x$. Therefore, a better understanding of the ODP mechanism (microkinetics) is essential to explore means of designing suitable catalysts and a suitable process environment.

Vanadium-based catalysts were intensively studied over years.[5−7] It is concluded that supported vanadium oxide catalysts are typically more selective than the unsupported bulk $V_2O_5$ material.[8−12] Several recent studies of the ODP reaction were dealt with $VO_x$ aggregates supported over mesoporous silica-based materials (MCM, SBA) with specific surface area of ca. 1000 $m^2/g$.[13−21] Propene yields up to 25% were achieved. Generally, the improving effect of the support material on catalytic performance of vanadia can be related to the following main factors: (1) supporting material helps to avoid the formation of nonselective $V_2O_5$ phase, (2) V−O−Me (Me is metal of the support) sites may be more selective than V−O−V ones, and (3) supporting material tunes acid−base properties of the resulting catalyst.[9,22−26] In general, strong acid properties decrease propene selectivity,[27] however, they can increase catalytic activity. Basic support can favor a better propene selectivity.[28,29]

Several other factors, such as reducibility of $VO_x$ species and their structure and their electronic properties, can influence both selective and nonselective reaction pathways in different directions at variation of vanadium loading or supporting material. Moreover, $VO_x$ species can cover acidic or basic sites of the support influencing the propene selectivity upon changing their concentration. Besides the above-mentioned selectivity-determining factors, it is also well-known that the overall performance of oxide materials in oxidative reactions is determined by the applied oxidizing agent. Monsanto performed a pilot plant study of the selective oxidation of benzene to phenol over Fe−ZSM-5 using $N_2O$ as oxidant.[30] In this case, the selectivity to phenol is considerably higher in comparison to using oxygen. A positive influence of $N_2O$ on product selectivity was also pointed out for the oxidative coupling of methane,[31,32] the selective oxidation of various aromatics to respective alcohols,[1] and the oxidative dehydrogenation of propane over Fe−ZSM-5 zeolites.[33−35] In our recent studies of the ODP reaction over

* To whom correspondence should be addressed. Phone: +49-30-63924448. Fax: +49 30 63924454. E-mail: evgenii@aca-berlin.de.

10.1021/jp070747c CCC: $37.00 © 2007 American Chemical Society
Published on Web 05/31/2007

alumina- and silica-supported vanadia catalysts,[20,36] it was demonstrated that propene selectivity increases upon replacing $O_2$ with $N_2O$. Since the ODP activity with $N_2O$ was lower than with $O_2$,[20] we suggested that the degree of reduction of $VO_x$ species might be important for achieving high propene selectivity.

On the basis of the above background, the present paper was aimed to provide new experimental insights into the governing factors concerning the superior performance of $N_2O$ as compared to $O_2$ in the ODP reaction over $VO_x/SiO_2$, $VO_x$/MCM-41, and $VO_x$/MCM-48. To this end, we performed in-situ UV/vis analysis under steady-state and transient conditions to experimentally determine the ability of $O_2$ and $N_2O$ for reoxidation of reduced $VO_x$ species. Moreover, the nature of active oxygen species involved in both selective and nonselective transformations of propane and propene was elucidated by means of transient isotopic experiments in the TAP (temporal analysis of products) reactor using isotopic traces.

## 2. Experimental Section

**2.1. Preparation of Catalytic Materials.** MCM-41, MCM-48, and $SiO_2$ were used as supporting materials for vanadium, with the latter being the catalytically active component. Vanadium loading was varied between 0.5 and 11.2 wt %. The mesoporous supports were prepared according to the procedure given in the literature,[20,37−40] while commercial amorphous $SiO_2$ was applied. The catalysts were prepared by impregnating the supports with a predetermined amount of vanadyl acetyl acetate ($[CH_3COCH{=}C(O-)CH_3]_2VO$) dissolved in toluene. The resulting catalyst precursor was subsequently subjected to drying at 400 K for 12 h and calcination in air at 823 K for 12 h. The total amount of vanadium was determined after the calcination of the samples. The catalysts are denoted below by their amount of vanadium loading (e.g., $VO_x$(2.7)/MCM-41 contains 2.7 wt % of V in the sample).

**2.2. Catalyst Characterization.** Nitrogen physisorption at 77 K was employed to obtain specific surface areas in a single-point BET analyzer (Gemini III 2375, Micromeritics). The method of Barret, Joyner, and Halenda (BJH) was employed to determine the pore size distribution.

Inductively coupled plasma (ICP) measurements were used to determine the vanadium concentrations of each catalyst after calcination at 823 K. The final vanadium content is presented in the brackets of the catalyst formula.

In-situ UV/vis experiments were performed at 773 K under steady-state and transient conditions. $BaSO_4$ was used as a white reference material. The UV/vis analysis was performed using an AVASPEC fiber optical spectrometer (Avantes) equipped with a DH-2000 deuterium-halogen light source and a CCD array detector. A high-temperature reflection probe consisting of six radiating and one reading optical fibers was located inside the furnace perpendicular to the reactor. The sensor was connected to the spectrometer, and the light source by fiber optical cables (length 2 m) consisting of a core of pure silica (diameter 0.4 mm) was coated with polyimide. The spectra were converted into the Kubelka−Munk function F(R). The position on the UV/vis fiber, the total flow, the reaction temperature, and the pressure were not changed upon switching from one to another reaction feed. Therefore, the observed changes in the UV/vis spectra relate exclusively to the change of the catalyst under different reaction conditions.

In steady-state UV/vis experiments, UV/vis spectra were recorded at 773 K in the range from 200 to 800 nm in $C_3H_8/O_2/Ne = 40/20/40$ or $C_3H_8/N_2O/Ne = 40/40/20$ flows.

In transient UV/vis experiments, UV/vis spectra (from 200 to 800 nm) and the Kubelka−Munk at 700 nm (d−d-transitions of reduced V-species) were recorded under different reaction conditions ($T = 773$ K, $C_3H_8/Ne = 40/60$, $H_2/N_2 = 5/95$, $N_2O/Ne = 40/60$, and $O_2/Ne = 20/80$) every 20 and 5 s, respectively. The temporal changes in the Kubelka function at 700 nm are related to the kinetics of reduction of oxidized $VO_x$ species and reoxidation of reduced $VO_x$ species upon feeding reducing and oxidizing agents, respectively.

In both modes, UV/vis spectra were taken at 773 K by passing feed mixtures through the catalyst bed. The total gas flow was kept at 40 $cm^3$ (STP)/min. Catalyst sieved fraction of 0.1−0.3 mm was used for these investigations. All these experimental conditions including the quartz-made reactor were very similar to those in catalytic continuous flow tests. The catalyst was slightly diluted (1:1−1:2) with quartz particles of the same particle size as the catalyst. A thermocouple inside the catalyst bed was used to control the reaction temperature. The gas composition at the reactor outlet during in-situ UV/vis experiments was controlled by online mass spectrometry (Balzer Omnistar). The propane and oxidant ($O_2$, $N_2O$) conversions were calculated from inlet and outlet concentration of these components. The following atomic mass units (AMUs) were analyzed: 44 ($CO_2$, $C_3H_8$), 42 ($C_3H_6$, $C_3H_8$), 32 ($O_2$), 30 ($N_2O$, $C_3H_8$), 29 ($C_3H_8$), 28 ($C_3H_8$, $C_3H_6$), 20 (Ne), and 18 ($H_2O$). The concentration of feed components and products was determined from the respective AMUs using fragmentation patterns and sensitivity factors, which arise from the different ionization probabilities of individual compounds. The relative sensitivities were determined as a ratio of the intensity of the mass spectrometry signal of each compound related to that of Ne (inert standard). The respective intensities were corrected according to the contribution of fragmentation pattern of other compounds to the measured AMU signal. The fragmentation patterns and respective sensitivities of feed components and reaction products were determined from separate calibration experiments, where a mixture of reference gas and inert standard was introduced into the reactor filled with $SiO_2$ particles.

**2.3. Transient Measurements.** To derive insights into reaction pathways of propane dehydrogenation to propene as well as of propane/propene oxidation to $CO_x$, transient experiments were performed in the temporal analysis of products (TAP-2) reactor using isotopic labels. The reactor setup has been described in detail elsewhere.[41] The catalytic material (30 mg; $d_p = 250-355$ $\mu$m) was placed between two layers of quartz of the same particle size in the microreactor made of quartz (40 mm long and 6 mm inner diameter). Prior to each transient experiment, the catalyst was pretreated in an oxygen flow for 1 h at 773 K and ambient pressure. The pretreated catalyst was then exposed to vacuum (ca. $10^{-5}$ Pa) before the pulse experiments were carried out at 773 K. Different gas mixtures ($C_3H_8/Ne = 1/1$, $C_3H_8/^{18}O_2/Ne = 2/1/2$) were pulsed over the catalyst, and the transient responses were monitored at atomic mass units (AMU) related to the feed components, reaction products, and inert gas. One pulse consisted of $10^{14}-5\cdot10^{14}$ molecules. Pulses were repeated for each AMU 10 times and were averaged to improve the signal-to-noise ratio. Ne (99.995), $^{18}O_2$ (95−98% of $^{18}O$, ISOTEC), and $C_3H_8$ (99.95) were used without additional purification. The variations in feed components and reaction products were determined from the respective AMUs using standard fragmentation patterns and sensitivity factors.

**2.4. Catalytic Tests.** The catalytic tests were performed in a U-shaped fixed bed quartz reactor (i.d. 5 mm) at atmospheric

pressure. The quartz reactor was immersed into a fluidized bed of quartz sand to provide isothermal operating conditions. A movable thermocouple inside the reactor tube was used for the measurement of the temperature inside the catalyst bed. The oxidative conversion of propane was investigated using feeds of 40 vol % $C_3H_8$ and 40 vol % $N_2O$ in Ne ($C_3H_8/N_2O/Ne$ = 40/40/20) or 40 vol % $C_3H_8$ and 20 vol % $O_2$ in Ne ($C_3H_8/O_2/Ne$ = 40/20/40) at 1 bar in the temperature range of 673−773 K. To determine product selectivity at different degrees of propane conversion, the total flow rate and the catalyst amount were varied from 30 to 240 $cm^3_{STP}\cdot min^{-1}$ and from 0.01 to 0.1 g, respectively. The product mixture was analyzed using online GC (HP 5890-II) equipped with Porapak Q and Molecular sieve-5 columns. The conversion of feed components, the selectivity, and the yield of reaction products were calculated from the inlet and outlet concentrations. To determine turnover frequency (TOF) of propane conversion, propane conversion was kept below 2%, that is, the catalytic reactor can be considered as a differential one. The turnover frequency was obtained as moles of propane converted per second per moles of vanadium assuming all vanadium sites are active.

Catalytic activity and product selectivity changed during the first 0.5−1.5 h on stream. After this time, a steady-state catalytic operation was achieved. Therefore, the concentrations of reaction products and feed components after 1.5−2 h on stream were taken for calculation reaction rates, conversion, and selectivity.

## 3. Results and Discussion

The results of physicochemical characterization of $VO_x/SiO_2$, $VO_x$/MCM-41, and $VO_x$/MCM-48 materials; their catalytic performance in the ODP reaction; and redox dynamics of $VO_x$ species from in-situ UV/vis analysis are presented in sections 3.1, 3.2, and 3.3, respectively. Thereafter, mechanistic aspects of $C_3H_6$ and $CO_x$ formation from transient experiments in the TAP reactor with isotopic traces are discussed. Finally (section 3.5), a reaction scheme of the ODP reaction is suggested, which explains the influence of oxidizing agent ($O_2$ vs $N_2O$) on selectivity and activity of differently structured $VO_x$ species supported over silica-based supports.

**3.1. Bulk and Surface Properties.** Since the results of our detailed physicochemical characterization (transmission electron microscopy (TEM), temperature-programmed reduction (TPR), UV/vis, Raman, and X-ray diffraction (XRD)) analysis of $VO_x$/MCM-41 materials have been previously published,[20] the most relevant results are briefly reported together with those for $VO_x/SiO_2$ and $VO_x$/MCM-48. These data are the basis of further elucidating some mechanistic aspects.

The BET values of unloaded MCM-41, MCM-48, and $SiO_2$ support materials amounted to 1040, 1049, and 300 $m^2/g$, respectively. Vanadium-loaded MCM-41 and $SiO_2$ materials showed a decrease in the specific surface area by a factor of ca. 20% for vanadium loadings up to 5.3 wt %. The $VO_x$(3.4)/MCM-48 catalyst lost ca. 50% of the original surface area of MCM-48. The average pore size of catalytic materials with vanadium loading below 10 wt % was calculated as ca. 2.7 and 4.1 nm for $VO_x$/MCM-41 and $VO_x$/MCM-48 materials, respectively. Thus, the mesoporous structure of the MCM-41 and MCM-48 supports was preserved in the synthesized catalytic materials (for MCM-41 it was proved previously by TEM in ref 20). The $S_{BET}$ value (52 $m^2/g$) of $VO_x$(11.2)/MCM-41 is significantly lower than those of the other catalysts. As reported in ref 20, the pore structure of MCM-41 is completely destroyed in this sample. Small $V_2O_5$ crystallites were observed in this sample by means of ex-situ XRD analysis. The XRD patterns of $VO_x$/MCM-48 and $VO_x/SiO_2$ with vanadium loading up to ca. 5 wt % do not show any signs of crystalline $V_2O_5$ phase. Additional UV/vis and Raman spectroscopic characterization studies (the data are not shown for brevity) did not indicate a possible presence of XRD-amorphous crystalline $V_2O_5$ nanoparticles for samples possessing up to 5.3 wt % vanadium.

To elucidate the distribution of surface $VO_x$ species, apparent surface densities of vanadium ($V/nm^2$) were calculated for all the studied catalysts using the BET values and vanadium loading. The calculated vanadium surface densities are 0.37, 0.6, 1.38, and 25.4 for $VO_x$(2.7)/MCM-41, $VO_x$(3.4)/MCM-48, $VO_x(2.9)/SiO_2$, and $VO_x$(11.2)/MCM-41, respectively. On the basis of the obtained densities and the literature[9] values for a vanadium monolayer (5−7 $V/nm^2$), it can be safely concluded that all catalytic materials, except for $VO_x$(11.2)/MCM-41, possess $VO_x$ species below one vanadium monolayer.

Further important information on the distribution of $VO_x$ species on the catalyst surface and their reducibility was obtained from $H_2$-TPR tests. The aim was to elucidate whether the structure (MCM-41, MCM-48, or amorphous silica) of silica support influences the redox properties of $VO_x$ species below one vanadium monolayer. A single maximum of $H_2$ consumption at ca. 801 and 806 K was observed upon reduction of $VO_x$(2.7)/MCM-41 and $VO_x$ (2.8)/$SiO_2$, respectively. The single $T_{max}$ temperature value may indicate the existence of $VO_x$ species of similar reducibility. Additionally to the maximal $H_2$ consumption at 810 K, a small shoulder at ca. 860 K was identified in the TPR profile of the $VO_x$(3.4)/MCM-48 sample. This shoulder becomes more pronounced for the $VO_x$(11.2)/MCM-41 sample, where crystalline $V_2O_5$ phase was identified by XRD analysis. According to the literature data,[37,42,43] the peak at 864 K could be due to the presence of highly polymerized $VO_x$ species or crystalline $V_2O_5$.

Summarizing the above discussion, it is concluded that the degree of polymerization of $VO_x$ species is influenced by the support material at apparent surface vanadium densities below one monolayer. The relative degree of polymerization of $VO_x$ species follows the order

$$VO_x(2.7)/MCM\text{-}41 < VO_x(2.8)/SiO_2 < VO_x(3.4)/MCM\text{-}48$$

The $VO_x$(11.2)/MCM-41 sample possesses microcrystalline $V_2O_5$ phase. The next section establishes correlations between the nature of $VO_x$ species and their performance in the ODP reaction with $O_2$ and $N_2O$.

**3.2. Catalytic Performance.** Catalytic performance of differently structured $VO_x$ species supported over MCM-41, $SiO_2$, and MCM-48 was determined using $C_3H_8/O_2/Ne$ = 40/20/40 and $C_3H_8/N_2O/Ne$ = 40/40/20 reaction mixtures. Since the amount of $N_2O$ was double that of $O_2$, both of the above reaction feeds contained the same amount of oxygen atoms. This allows the comparison of the influence of oxidizing agents on the ODP reaction. The TOF (turnover frequency) values of propane conversion in the presence of $O_2$ and $N_2O$ over $VO_x$ species below ($VO_x$(2.7)/MCM-41, $VO_x(2.8)/SiO_2$, and $VO_x$(3.4)/MCM-48) and above ($VO_x$(11.2)/MCM-41) one monolayer are compared in Table 1. The TOF values were calculated taking the total amount of vanadium atoms into account. This table illustrates that the catalytic activity of the $VO_x$(2.7)/MCM-41 catalyst is slightly higher than that of the $VO_x(2.8)/SiO_2$ and $VO_x$(3.4)/MCM-48 samples. This may be due to a lower degree of polymerization of $VO_x$ species over the $VO_x$(2.7)/MCM-41 catalyst as shown in section 3.1. The lowest TOF value was obtained over the $VO_x$(11.2)/MCM-41 sample, where microcrystalline $V_2O_5$ phase was detected. Irrespective of the

**TABLE 1: Turnover Frequencies (TOF) of Propane Conversion ($X(C_3H_8)$) and Ratios of $CO/C_3H_6$ and $CO_2/C_3H_6$ at Different Propane Conversions and 773 K Using $C_3H_8/O_2/Ne = 40/20/40$ and $C_3H_8/N_2O/Ne = 40/40/20$**

| samples | oxidants | TOF[a]/mol($C_3H_8$)·mol$_V^{-1}$·s$^{-1}$ | $X(C_3H_8) \sim 2\%$[b] | | $X(C_3H_8) \sim 10\%$[b] | |
|---|---|---|---|---|---|---|
| | | | $CO/C_3H_6$ | $CO_2/C_3H_6$ | $CO/C_3H_6$ | $CO_2/C_3H_6$ |
| $VO_x$(2.7)MCM-4 1 | $O_2$ | 0.016 | 0.09 | 0.07 | 0.18 | 0.13 |
| | $N_2O$ | 0.008 | 0.05 | 0.05 | 0.08 | 0.07 |
| $VO_x$(3.4)MCM-4 8 | $O_2$ | 0.011 | 0.13 | 0.08 | 0.38 | 0.19 |
| | $N_2O$ | 0.003 | 0.07 | 0.08 | 0.11 | 0.09 |
| $VO_x$(2.8)$SiO_2$ | $O_2$ | 0.011 | 0.08 | 0.09 | 0.51 | 0.35 |
| | $N_2O$ | 0.007 | 0.02 | 0.03 | 0.08 | 0.08 |
| $VO_x$(11.2)MCM-41 | $O_2$ | 0.002 | 1.7 | 0.27 | 5.1 | 1.7 |
| | $N_2O$ | 0.001 | 0.07 | 0.13 | 0.13 | 0.23 |

[a] The contact times for determining TOF values with $O_2$ and $N_2O$ were kept in the range 0.015−0.02 and 0.045−0.05 s·g·mL$^{-1}$, respectively. [b] To achieve degrees of propane conversion of 2 and 10%, the above contact times were increased by a factor of ca. 2 and ca.10, respectively.

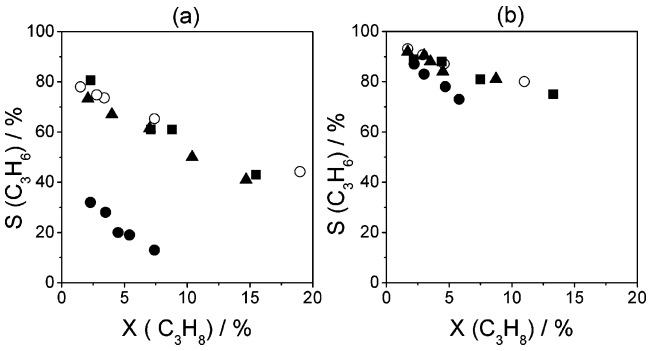


**Figure 1.** $C_3H_6$ selectivity over $VO_x$(2.7)/MCM-41 (○), $VO_x$(3.4)/MCM-48 (■), $VO_x$(2.8)/$SiO_2$ (▲), and $VO_x$(11)/MCM-41 (●) versus propane conversion at 773 K using $C_3H_8/O_2/Ne = 40/20/40$ (a) and $C_3H_8/N_2O/Ne = 40/40/20$ (b) mixtures.

structural difference of $VO_x$ species, the catalytic activity decreases when $O_2$ is replaced by $N_2O$.

For establishing overall mechanistic scheme of the ODP reaction with $O_2$ and $N_2O$ over $VO_x$ species of different degrees of polymerization, catalytic performance (product selectivity) was determined at different contact times, that is, different degrees of propane conversion. This knowledge is of high importance for catalyst designing, because it provides essential information on the sequence of product formation, that is, the catalyst ability for $C_3H_8$ conversion to $C_3H_6$ and $CO_x$ as well as for consecutive $C_3H_6$ combustion. The obtained selectivity−conversion relationships with $O_2$ are summarized in Figure 1. Propene selectivity decreases, while CO and $CO_2$ selectivities (the data are not shown) increase with an increase in the degree of propane conversion. Such behavior is explained by consecutive oxidation of the primarily formed propene to carbon oxides. For the $VO_x$(11.2)/MCM-41 sample, the low propene selectivity at near-to-zero degree of propane conversion is an indication for catalytic activity toward direct (not via consecutive propene oxidation) propane oxidation to carbon oxides. This reaction pathway does not play any significant role over other catalytic materials with vanadium loading below one monolayer. Over the latter catalysts, CO and $CO_2$ originate mainly via consecutive $C_3H_6$ oxidation.

We could not confirm a significant effect of morphology of the Si-based supports on alkene selectivity as reported in literature.[19,21,44] Only small differences in propene selectivity and total catalytic activity (Table 1) were found for highly dispersed $VO_x$ clusters supported over $SiO_2$, MCM-41, and MCM-48. The disagreement between the literature and the present data may be understood by taking the following discussion into consideration. The previous studies[19,21,44] were performed at 873 K, that is, 100 K higher than in the present study, where mass transport limitations cannot be completely excluded as mentioned in ref 19. Recently, Frank et al.[45] showed that mass transport strongly influences propene selectivity in the ODP reaction over highly dispersed $VO_x$ species over an alumina support. This is due to accumulation of propene inside the particle pores and its further oxidation. In contrast to the previous literature studies,[19,21,44] the present study was performed under conditions where mass transport phenomena are minimized. This may be a reason why the effect of the support morphology on propene selectivity could not be observed in our study.

Figure 1b illustrates selectivity−conversion relationships in the ODP reaction over differently structured $VO_x$ species using $N_2O$. As in the presence of $O_2$ (Figure 1a), propene selectivity decreases with an increase in propane conversion with $N_2O$, too. However, from the comparison of the results in Figure 1a and b, it is obvious that propene selectivity is higher with $N_2O$ than with $O_2$ over a broad range of degrees of propane conversion. This effect is more pronounced for the sample possessing microcrystalline $V_2O_5$. From a more detailed analysis of the data in Figure 1, the primary $C_3H_6$ selectivity (at near-to-zero degree of propane conversion) and the catalyst ability for consecutive $C_3H_6$ oxidation to $CO_x$ can be derived. These two parameters represent the catalyst activity for direct propane conversion to $CO_x$ and for consecutive combustion of primarily formed propene, respectively. In the present paper, the dependence of $S(C_3H_6)$ on $X(C_3H_8)$ at low propane conversion (<10%) is described by a linear function in eq 1.

$$S(C_3H_6) = -A \times X(C_3H_8) + S(C_3H_6)_{\text{primary}} \qquad (1)$$

where $S(C_3H_6)_{\text{initial}}$ and $A$ are the primary propene selectivity and the catalyst ability for consecutive propene oxidation to $CO_x$, respectively.

According to this function, the primary $C_3H_6$ selectivity is obtained from the intersect of the fitted line with the $S(C_3H_6)$ axis, while the slope of the line represents the catalyst ability for consecutive $C_3H_6$ oxidation to $CO_x$. This parameter is related to the catalyst activity for propene conversion to carbon oxides. The higher the slope of the function in eq 1, the faster the $CO_x$ production from $C_3H_6$. Establishing the relationships between the catalyst ability for consecutive propene oxidation and the structure of $VO_x$ species or the applied oxidizing agent is highly relevant for designing selective catalysts, since propene selectivity in the ODP reaction suffers mainly from the higher reactivity of propene as compared to propane. Figure 2 compares the primary $S(C_3H_6)$ and the catalyst ability ($A$) for consecutive $C_3H_6$ oxidation to $CO_x$ over differently structured $VO_x$ species in the presence of $O_2$ and $N_2O$.

For an $O_2$-containing reaction feed ($C_3H_8/O_2/Ne = 40/20/40$), it is clear that the primary propene selectivity is close for

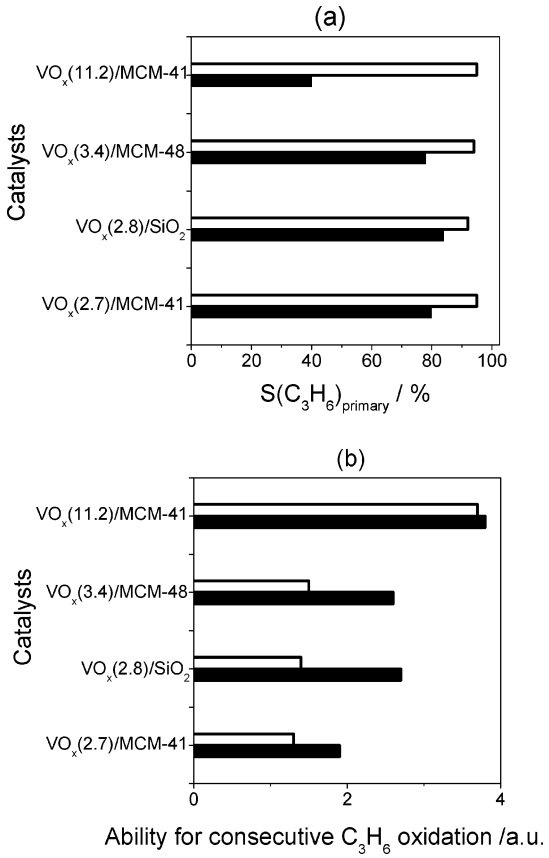


**Figure 2.** Primary $C_3H_6$ selectivity (a) and catalyst ability for consecutive $C_3H_6$ oxidation (b) at 773 K over $VO_x$(2.7)/MCM-41, $VO_x$(3.4)/MCM-48, $VO_x$(2.8)/$SiO_2$, and $VO_x$(11)/MCM-41 using $C_3H_8/O_2/Ne$ = 40/20/40 (solid bars) and $C_3H_8/N_2O/Ne$ = 40/40/20 (open bars) mixtures.

$VO_x$(2.7)/MCM-41, $VO_x$(3.4)/MCM-48, and $VO_x$(2.8)/$SiO_2$ materials but is significantly low over $VO_x$(11.2)/MCM-41 (Figure 2 a). From the characterization results in section 3.1, the latter material possesses microcrystalline $V_2O_5$ while other materials are free of microcrystalline $V_2O_5$ and possess highly dispersed two-dimensional $VO_x$ species. Figure 2b clearly demonstrates that consecutive propene oxidation is strongly influenced by the nature of $VO_x$ species, too. The following order of catalyst ability for propene oxidation was found:

$$VO_x(11.2)/MCM\text{-}41 > VO_x(3.4)/MCM\text{-}48 > VO_x(2.8)/SiO_2 > VO_x(2.7)/MCM\text{-}41$$

The degree of polymerization of $VO_x$ species follows the same order (section 3.1). Thus, the higher polymerized $VO_x$ species, the higher their activity for consecutive propene oxidation. This conclusion is in agreement with literature data[9] and with our recent results of the ODP reaction on $VO_x/\gamma\text{-}Al_2O_3$.[36]

Further insights into the influence of oxidizing agent on product selectivity in the ODP reaction are derived from the analysis of $CO/C_3H_6$ and $CO_2/C_3H_6$ ratios at different degrees of propane conversion. Table 1 represents these ratios at propane conversions of ca. 2 and 10%. For samples possessing highly dispersed $VO_x$ species, both of these ratios at a degree of propane conversion of ca. 2% decrease from ca. 0.1 to ca. 0.05 upon replacing $O_2$ with $N_2O$. However, the ratio of $CO_2/C_3H_6$ over polymerized $VO_x$ species increases from 0.04 to 0.13, while the ratio of $CO/C_3H_6$ decreases from 1.7 to 0.27, when $N_2O$ is used instead of $O_2$. For both oxidizing agents, the ratios of $CO/C_3H_6$ and $CO_2/C_3H_6$ increase with propane conversion, with the former increasing stronger. This increase is less pronounced for

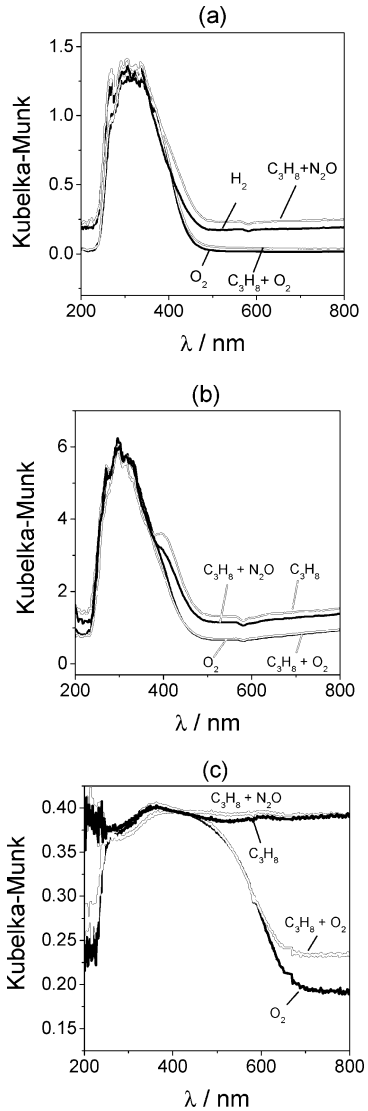


**Figure 3.** In-situ UV/vis spectra of $VO_x$(2.7)/MCM-41 (a), $VO_x$(2.8)/$SiO_2$ (b), and $VO_x$(11.2)/MCM-41 (c) under different reaction conditions at 773 K.

a feed with $N_2O$. This means that consecutive $C_3H_6$ oxidation to $CO_x$ (mainly to CO) is reduced in the presence of $N_2O$. This effect is more pronounced for polymerized $VO_x$ species.

Summarizing, two important improving effects of $N_2O$ on the ODP reaction should be especially emphasized: (1) a higher primary $C_3H_6$ selectivity (at near-to-zero degree of $C_3H_8$ conversion) is achieved and (2) lower activity for consecutive propene oxidation.

**3.3. In-Situ UV/Vis Analysis of Redox Behavior of $VO_x$ Species.** To elucidate possible reasons of the influence of oxidizing agent on the ODP performance of highly dispersed $VO_x$ species and microcrystalline $V_2O_5$, in-situ UV/vis measurements were performed at 773 K. The degrees of propane and oxidant ($O_2$ and $N_2O$) conversion were controlled by online mass spectrometry (MS). To ensure a near-to-uniform composition of the studied catalysts along the catalyst bed, propane and oxidant ($O_2$ or $N_2O$) conversions were kept below 5 and 10%, respectively.

Figure 3 exemplifies in-situ UV/vis spectra of $VO_x$(2.7)/MCM-41, $VO_x$(2.8)/$SiO_2$, and $VO_x$(11.2)/MCM-41 in oxidizing ($O_2/Ne$ = 20/80) and reducing ($H_2/N_2$ = 5/95 or $C_3H_8/Ne$ = 40/60) atmospheres as well as in ODP feeds ($C_3H_8/O_2/Ne$ =

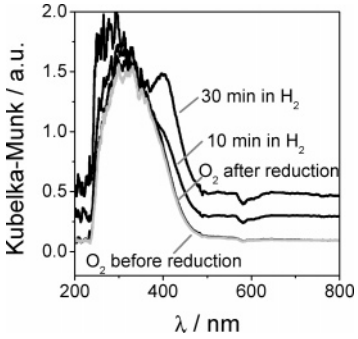


**Figure 4.** In-situ UV/vis spectra of $VO_x$(2.7)/MCM-41 in $O_2$ ($O_2$/Ne = 20/80) and $H_2$ ($H_2/N_2$ = 5/95) flows at 773 K.

40/20/40 or $C_3H_8/N_2O$/Ne = 40/40/20). The UV/vis spectrum in a flow of $O_2$ with the absorption at 295 nm is characteristic for tetrahedrally coordinated $V^{5+}O_x$ species. The adsorption in the 400−700 nm region (d−d transitions of reduced vanadium species) increases upon switching from an $O_2$ flow to a $H_2$ flow (Figure 3a); the UV/vis bands of $V^{4+}$ and $V^{3+}$ species appear as broad features in the 400−800 nm region (note the nonzero value of the absorption for the reduced samples in this region).[46,47] Similar changes were also observed when the oxidized catalyst was admitted to a $C_3H_8$ flow. Since no significant differences in the UV/vis spectra in $H_2$ and $C_3H_8$ flows were observed (Figure 3a), the effect of possible carbon-containing deposits in the case of $C_3H_8$ flow on the interpretation of UV/vis data can therefore be neglected.

Thus, the observed changes in the UV/vis spectra of $VO_x$-(2.7)/MCM-41 upon switching from oxidizing to reducing flows reflect the changes in reduction degree of $VO_x$ species under different reaction conditions. Taking the above discussion into account, the UV/vis spectra in $O_2$ (20% $O_2$ in Ne) and $C_3H_8$ (40% $C_3H_8$ in Ne) flows represent oxidized and reduced states of $VO_x$ species, respectively.

In the following, we compare UV/vis spectra under different ODP conditions ($C_3H_8/O_2$/Ne = 40/20/40 and $C_3H_8/N_2O$/Ne = 40/40/20) with the spectra of oxidized and reduced $VO_x$ species to derive insights into the reduction degree of $VO_x$ species under reaction conditions. One can see from Figure 3 that the UV/vis spectra during the ODP reaction with $O_2$ ($C_3H_8/O_2$/Ne = 40/20/40) and in an $O_2$ ($O_2$/Ne = 20/80) flow are very similar. This means that the oxidation state of $VO_x$ species in both cases is close to 5+. However, there is a strong difference between the UV/vis spectra in $O_2$ ($O_2$/Ne = 20/80) and $N_2O-C_3H_8$ ($N_2O/C_3H_8$/Ne = 40/40/20) flows, while the UV/vis spectra in $H_2$ ($H_2/N_2$ = 5/95) and $N_2O-C_3H_8$ ($N_2O/C_3H_8$/Ne = 40/40/20) flows are very similar. This evidence that the oxidation state of $VO_x$ species under conditions of the ODP reaction with $N_2O$ ($X(C_3H_8)$ < 5%, $X(N_2O)$ < 10%) is similar to the reduced one. This means that the oxidation state of vanadium in $VO_x$ species decreases from 5+ to 3+ and/or 4+ when the ODP reaction is performed with $N_2O$ instead of $O_2$.

Another interesting observation from Figure 3 is the appearance of a new band at 400−450 nm in the UV/vis spectrum of $VO_x$(2.8)/$SiO_2$ in a $C_3H_8$ ($C_3H_8$/Ne = 40/60) flow. A similar band was also identified over $VO_x$(2.7)/MCM-41 after 10−30 min on stream in $C_3H_8$. To prove whether this band may belong to carbon deposits, we performed time-on-stream in-situ UV/vis tests over $VO_x$(2.7)/MCM-41 in a $H_2$ flow ($H_2/N_2$ = 5/95). The results are shown in Figure 4. One can see that the band at 400−450 nm starts to appear after 10 min and becomes apparent after 30 min on stream in a $H_2$ flow. Since this band appears in the absence of carbon-containing species, its appearance due to coke deposition can be safely excluded. Possible origins of this band are discussed as follows. It is well-known that non-dehydrated $VO_x$/silica materials possess octahedral coordinated $VO_x$ species, in which adsorbed water is a ligand. On the basis of this experimental fact, it can be suggested that water is formed upon reaction of $VO_x$ species over $SiO_2$ and MCM-41 with $H_2$ and adsorbs over reduced $VO_x$ species increasing their coordination from tetrahedral to octahedral. However, to draw a more definitive conclusion about the origins of the band at 400−450 nm in $H_2$ at 773 K, new additional experiments are required.

It is also important to stress that there is no difference in the UV/vis spectra of $VO_x$ species under oxidizing conditions before and after treatments in $H_2$ (Figure 4). Similar results were obtained for all the oxidizing/reduction/reaction cycles described in Figure 3. This means that $VO_x$ species remain highly dispersed during the applied treatments and time-on-stream operation.

To check if $O_2$ and $N_2O$ show different ability (activity) for the reoxidation of reduced $VO_x$ species, in-situ UV/vis tests were performed in a transient mode. In these experiments, the oxidized sample was reduced in a flow of $C_3H_8$ ($C_3H_8$/Ne = 40/60) at 773 K for 10 min followed by flushing in a Ne flow for 1 min and feeding an $O_2$ flow ($O_2$/Ne = 20/80) over the reduced catalyst. The sample was kept in this flow for 30 min to reoxidate reduced $VO_x$ species. Hereafter, the reoxidized catalyst was again reduced in $C_3H_8$ followed by its reoxidation in a $N_2O$ ($N_2O$/Ne = 40/60) flow. In all the above experiments, UV/vis spectra from 200 to 800 nm and Kubelka−Munk at 700 nm were recorded every 20 and 5 s, respectively. The respective results are summarized in Figure 5 and Figure 6.

It is clear from Figure 5 that there is no significant difference in the spectra of fully oxidized $VO_x$ species and $VO_x$ species having been reoxidized for 5 s in an $O_2$ flow after $C_3H_8$ pretreatment. As compared to $O_2$, reoxidation of reduced $VO_x$ species with $N_2O$ is slower, since these species are fully oxidized after ca. 30 s on steam in $N_2O$.

More detailed insights into the kinetics of reduction of oxidized $VO_x$ species by $C_3H_8$ and reoxidation of reduced ones by $O_2$ and $N_2O$ were derived from the analysis of temporal changes in the Kubelka−Munk function in Figure 6. At time zero, we switched from an $O_2$ flow ($O_2$/Ne = 20/80) to a $C_3H_8$ flow ($C_3H_8$/Ne = 40/60). As result, the Kubelka−Munk function at 700 nm increases from 0 (fully oxidized $VO_x$ species) and reaches a constant value of ca. 0.2 after 5 min on $C_3H_8$ stream. Similar changes were observed when $H_2$ was used as a reducing agent instead of $C_3H_8$. Therefore, we can safely conclude that the observed changes are due to the reduction of oxidized $VO_x$ species by propane and are not due to deposition of carbon-containing species in the case of $C_3H_8$. To prove whether the reduction/reoxidation of $VO_x$ species is a reversible process, an $O_2$ flow ($O_2$/Ne = 20/80) was fed over the reduced sample (at ca. 10 min in Figure 6) followed by $C_3H_8$ feeding (at ca. 22 min in Figure 6).

As shown in Figure 6, the Kubelka−Munk function at 700 nm falls from ca. 0.2 to 0 after a few seconds in the $O_2$ flow and reversibly increases to 0.2 in the $C_3H_8$ flow. Two important conclusions were derived: (1) reduction/oxidation of $VO_x$ species is a reversible process and (2) reduction of oxidized $VO_x$ species by $C_3H_8$ is slower than reoxidation of reduced $VO_x$ species by $O_2$. When $N_2O$ was used for the reoxidation of reduced $VO_x$ species (ca. 32−40 min in Figure 6), these species were also reoxidized. However, the temporal changes in the Kubelka−Munk function at 700 nm are slower than those with $O_2$. From this difference in the temporal profiles,

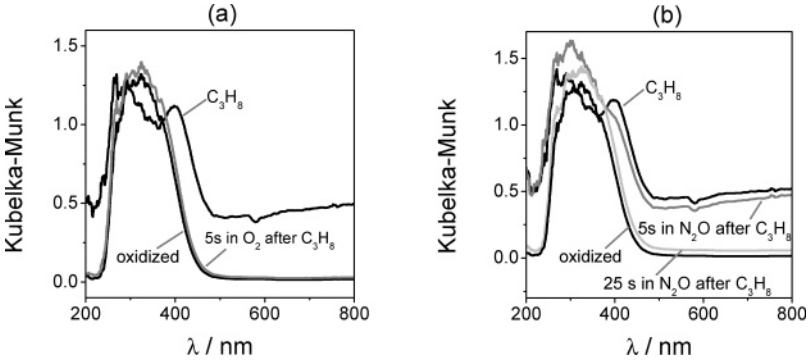


**Figure 5.** In-situ UV/vis spectra of $VO_x$(2.7)/MCM-41 at 773 K during $O_2-C_3H_8-O_2$ (a) and $O_2-C_3H_8-N_2O$ (b) cycles: $O_2$/Ne = 20/80, $C_3H_8$/Ne = 40/60, and $N_2O$/Ne = 40/60.

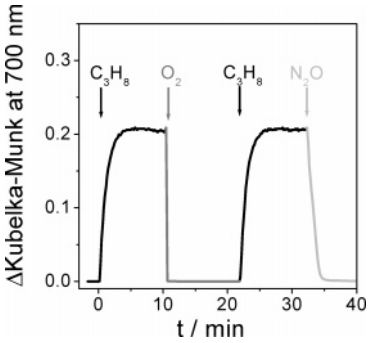


**Figure 6.** Temporal changes in Kubelka−Munk function at 700 nm during a $C_3H_8-O_2-C_3H_8-N_2O$ redox sequence over $VO_x$(2.7)/MCM-41 at $T$ = 773 K. The catalyst was pretreated in $O_2$ at 773 K before the sequence. $O_2$/Ne = 20/80, $C_3H_8$/Ne = 40/60, and $N_2O$/Ne = 40/60.

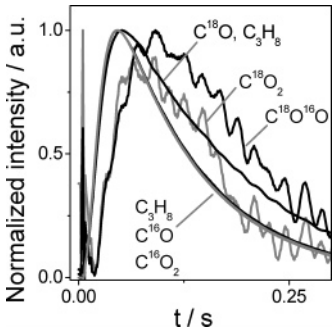


**Figure 7.** Height-normalized transient responses of $CO_x$ products obtained in the TAP reactor upon $C_3H_8$−Ne ($C_3H_8/^{18}O_2$/Ne = 2/1/2) pulsing over $VO_x$(2.7)/MCM-41 at 773 K.

it is concluded that the reoxidation of reduced $VO_x$ species by $N_2O$ is slower than by $O_2$. Similar results were obtained for other catalytic materials studied. Taking the difference in the oxidizing ability of $O_2$ and $N_2O$, it is easy to understand why the average oxidation state of $VO_x$ species under $C_3H_8-O_2$ conditions is higher than under $C_3H_8-N_2O$ (Figure 6). The lower ability of $N_2O$ for reoxidation of reduced $VO_x$ species is also responsible for the lower ODP activity with $N_2O$ than with $O_2$ as was previously suggested for $VO_x$/MCM-41[20] and $VO_x/\gamma$-$Al_2O_3$[36] catalytic materials.

**3.4. Mechanistic Aspects of Product Formation under Transient Conditions.** The effect of oxygen species (lattice oxygen or adsorbed) on the ODP reaction was studied by pulsing a mixture of propane and labeled oxygen ($^{18}O_2$) over the catalyst, which was preoxidized by $^{16}O_2$. $CO_x$ products containing different oxygen isotopes ($^{16}O$ and $^{18}O$) were detected at the reactor outlet. Their transient responses are presented in Figure 7 in a height-normalized form for better comparison of their pulse shapes. The presence of $^{16}O$ (not pulsed gas-phase oxygen) in CO and $CO_2$ evidences the participation of lattice oxygen of $VO_x$ species in combustion of $C_3H_8/C_3H_6$. This result is very similar to previous reported ones over various vanadium-based catalytic materials.[27,48,49]

Since transient responses of carbon oxides contain both labeled ($^{18}O$) and nonlabeled ($^{16}O$) oxygen species (Figure 7), two independent reaction pathways in $CO_x$ formation can be suggested: (1) with participation of labeled (adsorbed) and (2) nonlabeled (lattice) oxygen. However, the concentration of $CO_2$ and CO formed with participation of labeled oxygen ($C^{18}O_2$, $C^{18}O^{16}O$, and $C^{18}O$) was significantly lower than $C^{16}O_2$ and $C^{16}O$. This indicates that $C^{16}O$ and $C^{16}O_2$ are the main $CO_x$ products. In other words, lattice oxygen of $VO_x$ species is mainly responsible for $CO_x$ formation. Adsorbed oxygen species formed from gas-phase labeled ($^{18}O_2$) oxygen play only a minor role in $CO_x$ formation under transient vacuum conditions. This may be because the concentration of lattice nonlabeled oxygen in $VO_x$ species is considerably higher than that of labeled oxygen in the $C_3H_8-^{18}O_2$ pulse. The ratio of vanadium to the amount of $^{18}O_2$ in one pulse was estimated as ca. $5\cdot10^4$. However, the contribution of adsorbed oxygen species to the formation of $CO_x$ can be significantly higher under ambient-pressure conditions. We would like to emphasize that no labeled oxygen species in $CO_x$ was observed in our previous experiments over $VO_x/\gamma$-$Al_2O_3$ under similar conditions in the TAP reactor.[27] This can be explained by the fact that incorporation of gas-phase oxygen into $VO_x$ species occurs considerably faster over $VO_x/\gamma$-$Al_2O_3$ as compared to $SiO_2$-based catalysts. This assumption is indirectly supported by the recently reported results of the ODP reaction over $VO_x/Al_2O_3$[50] and $VO_x/SiO_2$[51] in cofeed ($O_2$ and $C_3H_8$ are fed together) and cyclic ($O_2$ and $C_3H_8$ are fed separately and periodically) modes. No substantial differences in propene selectivity between the cofeed and cyclic conditions were found over the alumina-based catalysts, while propene selectivity over the silica-based one was significantly improved when the ODP reaction was performed under the cyclic conditions. In the latter case, the negative effect of adsorbed oxygen species on propene selectivity could be avoided.

**3.5. Role of Oxidizing Agent in the ODP Reaction.** The results of steady-state ODP studies suggest a complex reaction scheme of parallel and consecutive steps for the ODP reaction using either $O_2$ or $N_2O$. According to this scheme, $C_3H_8$ is directly converted to $C_3H_6$ and $CO_x$, with the latter reaction path playing a significant role for $VO_x$(11.2)/MCM-41 sample possessing microcrystalline $V_2O_5$. The formed propene is further converted to CO and $CO_2$. The importance of direct (not via consecutive propene oxidation) propane and consecutive propene oxidation to $CO_x$ is significantly higher in the presence of $O_2$ than in $N_2O$. Hence, the catalytic performance is determined by the oxidant activation.

Combining the results of in-situ UV/vis analysis and transient isotopic experiments with catalytic data, two important conclusions about the role of $O_2$ and $N_2O$ in the ODP reaction were derived: (1) the ability of oxidant for reoxidation of reduced $VO_x$ species and (2) the nature of selective and nonselective oxygen species. The former oxidant property tunes the degree of reduction of vanadium species; the lower the oxidizing ability, the higher the reduction degree of $VO_x$ species. This is essential for achieving high primary propene selectivity and for suppressing consecutive propene oxidation to CO and $CO_2$ as shown in Figure 2. This improving effect of $N_2O$ is related to spatial separation of active lattice oxygen species, that is, to reducing surface density of active oxygen species. Since 7−10 oxygen atoms are required for $CO_x$ formation from propane/propene but only one for propene formation, nonselective propane/propene oxidation to $CO_x$ will be inhibited upon increasing degree of reduction of $VO_x$ species. However, the degree of reduction of $VO_x$ species is not the only reason for superior performance of $N_2O$ as compared to $O_2$. On the basis of the results of transient isotopic experiments in section 3.4, it is suggested that the nature of oxygen species influences also the $CO_x$ formation. It is well-known[52] that $O_2$ adsorption over reducible metal oxides occurs via a complex sequence of redox processes until $O^{2-}$ (lattice oxygen) is formed. Density functional theory (DFT) calculations predict that gas-phase oxygen adsorbs molecularly over anion vacancy of reduced $VO_x$ species.[53,54] This biatomic adsorbed oxygen dissociates further yielding lattice oxygen species. Adsorbed (nonlattice) oxygen species were suggested to be nonselective ones for the ODP reaction over V−Mg−O[55,56] and $Mn_{0.18}V_{0.3}Cr_{0.23}W_{0.26}O_x$−$Al_2O_3$[57] catalytic materials. In contrast to $O_2$ adsorption, $N_2O$ decomposition over reducible metal oxides yields mononuclear oxygen species: $O^-$ or $O^{2-}$, which are considered as selective ones.[52] Further experimental mechanistic studies and theoretical (density functional theory) calculations are in progress with the aim to precisely define the nature of oxygen species originating from $O_2$ and $N_2O$ over reduced $VO_x$ species.

## 4. Summary and Conclusions

Experimental insights into the possible origins of superior performance of $N_2O$ as compared to $O_2$ in the oxidative dehydrogenation of propane over $VO_x/SiO_2$, $VO_x$/MCM-41, and $VO_x$/MCM-48 were derived from in-situ UV/vis analysis in combination with transient isotopic studies in the temporal analysis of products reactor. The in-situ UV/vis spectroscopy evidenced a higher degree of reduction of $VO_x$ species under $C_3H_8$−$N_2O$ than $C_3H_8$−$O_2$ conditions. By using this method in a transient mode, the ability of $O_2$ and $N_2O$ for reoxidation of reduced $VO_x$ species was experimentally distinguished; $N_2O$ reoxidizes reduced $VO_x$ species slower than $O_2$. Besides influencing the reduction degree of $VO_x$ species, $N_2O$ does not produce nonselective adsorbed oxygen species (possibly of biatomic nature), which are formed from $O_2$ and catalyze nonselective consecutive propene oxidation to $CO_x$.

**Acknowledgment.** Support by Deutsche Forschungsgemeinschaft (DFG) within the frame of the competence network (Sonderforschungsbereich 546) "Structure, dynamics and reactivity of transition metal oxide aggregates" has been greatly appreciated. The authors would like to thank Olga Schulz for technical assistance.

## References and Notes

(1) Panov, G. I. *CatTech* **2000**, *4*, 18.
(2) Hutchings, G. J.; Scurrell, M. S. *CatTech* **2003**, *7*, 90.
(3) Buyevskaya, O. V.; Baerns, M. *Catalysis* **2002**, *16*, 155.
(4) Baerns, M.; Grubert, G.; Kondratenko, E. V.; Linke, D.; Rodemerk, U. *Oil Gas-Eur. Mag.* **2003**, *1*, 36.
(5) Cavani, F.; Trifiro, F. *Catal. Today* **1995**, *24*, 307.
(6) Mamedov, E. A.; Corberan, V. C. *Appl. Catal. A* **1995**, *127*, 1.
(7) Kung, H. H. *Adv. Catal.* **1994**, *40*, 1.
(8) Wachs, I. E.; Weckhuysen, B. M. *Appl. Catal. A* **1997**, *157*, 67.
(9) Blasco, T.; López Nieto, J. M. *Appl. Catal. A* **1997**, *157*, 117.
(10) Argyle, M. D.; Chen, K.; Bell, A. T.; Iglesia, E. *J. Catal.* **2002**, *208*, 139.
(11) Chen, K.; Bell, A. T.; Iglesia, E. *J. Catal.* **2002**, *209*, 35.
(12) Weckhuysen, B. M.; Keller, D. E. *Catal. Today* **2003**, *78*, 25.
(13) López Nieto, J. M. *Top. Catal.* **2001**, *15*, 189.
(14) Buyevskaya, O. V.; Brückner, A.; Kondratenko, E. V.; Wolf, D.; Baerns, M. *Catal. Today* **2001**, *67*, 369−378.
(15) Solsona, B.; Blasco, T.; López Nieto, J. M.; Pena, M. L.; Rey, F.; Vidal-Moya, A. *J. Catal.* **2001**, *203*, 443−452.
(16) Wang, Y.; Zhang, Q.; Ohishi, Y.; Shishido, T.; Takehira, K. *Catal. Lett.* **2001**, *72*, 215.
(17) Zhang, Q.; Wang, Y.; Ohishi, Y.; Shishido, T.; Takehira, K. *J. Catal.* **2001**, *202*, 308.
(18) Santamaria-Gonzalez, J.; Luque-Zambrana, J.; Merida-Robles, J.; Maireles-Torres, P.; Rodriguez-Castellon, E.; Jimenez-Lopez, A. *Catal. Lett.* **2000**, *68*, 67.
(19) Liu, Y.-M.; Cao, Y.; Yi, N.; Feng, W.-L.; Dai, W.-L.; Yan, S.-R.; He, H.-Y.; Fan, K.-N. *J. Catal.* **2004**, *224*, 417.
(20) Kondratenko, E. V.; Cherian, M.; Baerns, M.; Su, X.; Schlögl, R.; Wang, X.; Wachs, I. E. *J. Catal.* **2005**, *234*, 131.
(21) Liu, Y.-M.; Feng, W.-L.; Li, T.-C.; He, H.-Y.; Dai, W.-L.; Huang, W.; Cao, Y.; Fan, K.-N. *J. Catal.* **2006**, *239*, 125.
(22) Gervasini, A.; Carniti, P.; Keranen, J.; Niinisto, L.; Auroux, A. *Catal. Today* **2004**, *96*, 187.
(23) Keranen, J.; Auroux, A.; Ek, S.; Niinisto, L. *Appl. Catal. A* **2002**, *228*, 213.
(24) Le Bars, J.; Auroux, A.; Forissier, M.; Vedrine, J. C. *J. Catal.* **1996**, *162*, 250.
(25) Wachs, I. E.; Jehng, J.-M.; Deo, G.; Weckhuysen, B. M.; Guliants, V. V.; Benziger, J. B.; Sundaresan, S. *J. Catal.* **1997**, *170*, 75.
(26) Khodakov, A.; Olthof, B.; Bell, A. T.; Iglesia, E. *J. Catal.* **1999**, *181*, 205.
(27) Kondratenko, E. V.; Steinfeldt, N.; Baerns, M. *Phys. Chem. Chem. Phys.* **2006**, *8*, 1624.
(28) Pak, C.; Bell, A. T.; Tilley, T. D. *J. Catal.* **2002**, *206*, 49.
(29) Garcia Cortez, G.; Fierro, J. L. G.; Banares, M. A. *Catal. Today* **2003**, *78*, 219.
(30) Uriatre, A. K. *Stud. Surf. Sci. Catal.* **2000**, *130*, 743.
(31) Yamamoto, H. Y.; Chu, H. Y.; Xu, M.; Shi, C.; Lunsford, J. *J. Catal.* **1993**, *142*, 325.
(32) Kondratenko, E. V.; Maksimov, N. G.; Selyutin, G. E.; Anshits, A. G. *Catal. Today* **1995**, *24*, 273.
(33) Nowinska, K.; Waclaw, A.; Izbinska, A. *Appl. Catal. A* **2003**, *243*, 225.
(34) Pérez-Ramírez, J.; Kondratenko, E. V. *Chem. Commun.* **2003**, 2152.
(35) Kondratenko, E. V.; Pérez-Ramírez, J. *Appl. Catal. A* **2004**, *267*, 181.
(36) Kondratenko, E.; Cherian, M.; Baerns, M. *Catal. Today* **2006**, *112*, 60.
(37) Grubert, G.; Rathousky, J.; Schulz-Ekloff, G.; Wark, M.; Zukal, A.; *Microporous Mesoporous Mater.* **1998**, *22*, 225.
(38) Pickup, D. M.; Mountjoy, G.; Wallidge, G. W.; Anderson, R.; Cole, J. M.; Newport, R. J.; Smith, M. E. *J. Mater. Chem.* **1999**, *9*, 1299.
(39) Baltes, M.; Cassiers, K.; Van Der Voort, P.; Weckhuysen, B. M.; Schoonheydt, R. A.; Vansant, E. F. *J. Catal.* **2001**, *197*, 160.
(40) Sun, J.-H.; Coppens, M.-O. *J. Mater. Chem.* **2002**, *12*, 3016.
(41) Gleaves, J. T.; Yablonsky, G. S.; Phanawadee, P.; Schuurman, Y. *Appl. Catal. A* **1997**, 160, 55.
(42) Kanervo, J. M.; Harlin, M. E.; Krause, A. O. I.; Banares, M. A. *Catal. Today* **2003**, *78*, 171.
(43) Ferreira, M. L.; Volpe, M. U. *J. Mol. Catal. A* **2002**, *184*, 349.
(44) Kucherov, A. V.; Ivanov, A. V.; Kucherova, T. N.; Nissenbaum, V. D.; Kustov, L. M. *Catal. Today* **2003**, *81*, 297.
(45) Frank, B.; Dinse, A.; Ovsitser, O.; Kondratenko, E. V.; Schomäcker, R. *Appl. Catal. A* **2007**, *323*, 66.
(46) Baltes, M.; Cassiers, K.; Van Der Voort, P.; Weckhuysen, B. M.; Schoonheydt, R. A.; Vansant, E. F. *J. Catal.* **2001**, *197*, 160.
(47) Gao, X.; Bare, S. R.; Weckhuysen, B. M.; Wachs, I. E. *J. Phys. Chem. B* **1998**, *102*, 10842.
(48) Buyevskaya, O. V.; Baerns, M. *Catal. Today* **1998**, *42*, 315.
(49) Pantazidis, A.; Bucholz, S. A.; Zanthoff, H. W.; Schuurman, Y.; Mirodatos, C. *Catal. Today* **1998**, *40*, 207.
(50) Ballarini, N.; Cavani, F.; Cericola, A.; Cortelli, C.; Ferrari, M.; Trifiro, F.; Capannelli, G.; Comite, A.; Catani, R.; Cornaro, U. *Catal. Today* **2004**, *91*−*92*, 99.

(51) Ballarini, N.; Cavani, F.; Ferrari, M.; Catani, R.; Cornaro, U. *J. Catal.* **2003**, *213*, 95.

(52) Bielanski, A.; Haber, J. *Oxygen in Catalysis*; Marcel Dekker: New York, 1991; p 320.

(53) Hermann, K.; Witko, M. Theory of physical and chemical behavior of transitionmetal oxides: vanadium and molybdenum oxides. In *The Chemical Physics of Solid Surfaces*; Woodruff, D. P., Ed.; Elsevier Science: Amsterdam, 2001; p 136.

(54) Tokarz-Sobieraj, R.; Witko, M.; Grybos, R. *Catal. Today* **2005**, *99*, 241.

(55) Zanthoff, H. W.; Buchholz, S. A.; Pantazidis, A.; Mirodatos, C. *Chem. Eng. Sci.* **1999**, *54*, 4397.

(56) Creaser, D.; Andersson, B.; Hudgins, R. R.; Silveston, P. L. *J. Catal.* **1999**, *182*, 264.

(57) Kondratenko, E. V.; Cherian, M.; Baerns, M. *Catal. Today* **2005**, *99*, 59.